HHS Public Access

Author manuscript

Clin Cancer Res. Author manuscript; available in PMC 2016 February 23.

Published in final edited form as:

Clin Cancer Res. 2015 September 1; 21(17): 3906–3912. doi:10.1158/1078-0432.CCR-14-2546.

MR-Guided Near-Infrared Spectral Tomography Increases Diagnostic Performance of Breast MRI

Michael A. Mastanduno[1], **Junqing Xu**[2], **Fadi El-Ghussein**[1], **Shudong Jiang**[1], **Hong Yin**[2], **Yan Zhao**[1], **Ke Wang**[2], **Fang Ren**[2], **Jiang Gui**[3], **Brian W. Pogue**[1], and **Keith D. Paulsen**[1,4]

[1]Thayer School of Engineering, Dartmouth College, Hanover, New Hampshire

[2]Department of Radiology, Xijing Hospital, Xi'an, China

[3]Department of Community and Family Medicine, Geisel School of Medicine, Dartmouth College, Hanover, New Hampshire

[4]Department of Diagnostic Radiology, Geisel School of Medicine, Dartmouth College, Hanover, New Hampshire

Abstract

Purpose—The purpose of this study was to determine the diagnostically most important molecular biomarkers quantified by magnetic resonance-guided (MR) near-infrared spectral tomography (NIRST) that distinguish malignant breast lesions from benign abnormalities when combined with outcomes from clinical breast MRI.

Experimental Design—The study was HIPAA compliant and approved by the Dartmouth Institutional Review Board, the NIH, the United States State Department, and Xijing Hospital. MR-guided NIRST evaluated hemoglobin, water, and lipid content in regions of interest defined by concurrent dynamic contrast-enhanced MRI (DCE-MRI) in the breast. MRI plus NIRST was performed in 44 subjects (median age, 46, age range, 20–81 years), 28 of whom had subsequent malignant pathologic diagnoses, and 16 had benign conditions. A subset of 30 subject

Corresponding Authors: Keith D. Paulsen, Dartmouth College, 14 Engineering Drive, Hanover, NH 03755. Phone: 603-646-3860; Fax: 603-646-3856; keith.paulsen@dartmouth.edu; and Hong Yin, Department of Radiology, Xijing Hospital, 127 West Changle Road, Xi'an 710032, China, Phone: 86-29-84775421; yinhong@fmmu.edu.cn.
Current address for Michael A. Mastanduno: Clark Center, 318 Campus Drive, Room E150, Stanford, CA 94305
M.A. Mastanduno and J. Xu contributed equally to the article.

Note: Supplementary data for this article are available at Clinical Cancer Research Online (http://clincancerres.aacrjournals.org/).

Disclosure of Potential Conflicts of Interest
No potential conflicts of interest were disclosed.

Authors' Contributions
Conception and design: M.A. Mastanduno, F. El-Ghussein, S. Jiang, H. Yin, B.W. Pogue, K.D. Paulsen
Development of methodology: M.A. Mastanduno, J. Xu, F. El-Ghussein, S. Jiang, B.W. Pogue, K.D. Paulsen
Acquisition of data (provided animals, acquired and managed patients, provided facilities, etc.): M.A. Mastanduno, J. Xu, F. El-Ghussein, S. Jiang, H. Yin, Y. Zhao, K. Wang, F. Ren
Analysis and interpretation of data (e.g., statistical analysis, biostatistics, computational analysis): M.A. Mastanduno, J. Xu, S. Jiang, H. Yin, K. Wang, J. Gui, K.D. Paulsen
Writing, review, and/or revision of the manuscript: M.A. Mastanduno, J. Xu, S. Jiang, H. Yin, B.W. Pogue, K.D. Paulsen
Administrative, technical, or material support (i.e., reporting or organizing data, constructing databases): M.A. Mastanduno, J. Xu, S. Jiang Study supervision: H. Yin, K.D. Paulsen
Other (checked "Analysis and interpretation" and was involved with the interpretation of the data, but not its analysis *per se*): K.D. Paulsen

examinations yielded optical data that met minimum sensitivity requirements to the suspicious lesion and were included in the analyses of diagnostic performance.

Results—In the subset of 30 subject examinations meeting minimum optical data sensitivity criterion, the MR-guided NIRST separated malignant from benign lesions using total hemoglobin (HbT; $P < 0.01$) and tissue optical index (TOI; $P < 0.001$). Combined MRI plus TOI data caused one false positive and 1 false negative, and produced the best diagnostic performance, yielding an AUC of 0.95, sensitivity of 95%, specificity of 89%, positive predictive value of 95%, and negative predictive value of 89%, respectively.

Conclusions—MRI plus NIRST results correlated well with histopathologic diagnoses and could provide additional information to reduce the number of MRI-directed biopsies.

Introduction

Diagnostic radiologic evaluations of the breast are based on anatomical structures observed in mammography and ultrasonography, and vascular leakage of injected contrast in MRI. Molecular or cellular information obtained at the time of imaging could influence the process of recommending biopsy and positively impact patients by minimizing the emotional and financial costs of unnecessary procedures due to false-positive imaging results. Novel optical imaging systems that monitor key molecules and cellular activity related to tissue physiology exist and are in various stages of technical evaluation. MR-guided near-infrared spectral tomography (NIRST) is an emerging approach that could benefit patients after their initial screening (1) by increasing the specificity of breast MRI through the addition of a concurrent optical scan prior to the biopsy decision (2). The technique noninvasively quantifies oxy- and deoxy-hemoglobin concentration, water and lipid content, and scattering parameters in adipose, fibroglandular, and tumor tissues. Derived parameters such as tissue optical index (TOI), which combine these image indicators into a single measure, are also possible (3). Hundreds of patients have undergone optical breast imaging examinations at multiple academic centers in the United States and Europe with promising results in larger tumors that are more superficially located (4–6). Because MRI information can guide optical image reconstruction, the MR-guided NIRST technique has the potential to improve the depth at which smaller lesions can be characterized relative to stand-alone optical imaging systems (7).

Ntziachristos and colleagues (8) and then Brooksby and colleagues (9) reported combined MRI/optical tomography systems where concurrent MRI and optical imaging was performed to increase the information available from clinical breast MRI examinations. Advances in these systems now allow MRI-guided recovery of the optical parameters in locally defined regions within the breast to estimate accurate molecular and cellular contrast from multiwavelength spectroscopy (8, 9). While the approach has shown distinctions between malignant and benign lesions in case studies, it has not been evaluated in a larger patient population. In this study, 44 women with breast abnormalities of unknown diagnoses scheduled for surgical resection were imaged to estimate the diagnostic value of MR-guided NIRST when used to characterize suspicious regions identified by dynamic contrast-enhanced MRI (DCE-MRI). The multimodality breast examinations in 14 of these subjects yielded optical data that did not meet minimum lesion sensitivity criterion (10), and were

excluded from the final analysis of the remaining 30 subjects. Abnormalities were characterized relative to the background breast as either malignant or benign, and scored versus the subsequent pathologic diagnosis. Results from these examinations were used to generate sensitivity and specificity for receiver operating curve (ROC) analysis. Individual case studies are presented along with analyses of the composite data to illustrate the potential of combined MRI and NIRST as an alternative that increases the specificity of clinical breast MRI as presently practiced without reducing its sensitivity.

Materials and Methods

Patient characteristics

The study protocol for human subject imaging was approved by the Committee for the Protection of Human Subjects at Dartmouth-Hitchcock Medical Center and at Xijing Hospital (Xi'an, China). The trial was conducted with federal support and, as a result, also required approval from the U.S. State Department in addition to the NIH. All patients were recruited from Xijing Hospital and provided written consent after the nature of the procedure was fully explained by their referring physician. Specifically, subjects were recruited for imaging by several breast surgeons in Xijing Hospital. Each individual continued to surgery following the MRI/NIRST examination as part of their scheduled standard-of-care treatment at the hosting institution. Patients were selected based on eligibility criteria, which included having at least one suspected breast abnormality and no contraindications for undergoing breast MRI. Patients who underwent a biopsy procedure within 10 days prior to the MRI/NIRST examination date were excluded from the study due to the possible presence of contusions or bleeding at the biopsy site that could alter or influence the imaging findings (6, 11).

All disease was confirmed by histopathologic analysis of tissue removed during surgery. Subjects were female, ages 20 to 81 years old. Within the group of women with malignant pathology, the mean age was 49 ± 11 years (range, 24–81 years), whereas the mean age was 37 ± 10 years (range, 20–51 years) for women with pathologically confirmed benign conditions, which was significantly less than the mean age of the malignant enrollments ($P < 0.001$). Patient BMI had a mean of 23.0 with standard deviation of 3.4. Breast sizes of all patients were distributed as follows: 16 A-cup, 15 B-cup, 10 C-cup, and 3 D-cup. Because most patients did not have prior mammography, breast density was assessed by an experienced breast radiologist from the T1 MRI and categorized as follows: 5 fatty, 16 scattered, 12 heterogeneously dense, and 11 extremely dense. Sixteen subjects were postmenopausal, whereas 28 were premenopausal. Table 1 summarizes means, standard deviations, and ranges for subject characteristics by pathologic diagnosis.

Optical imaging system

The MRI/NIRST system deployed in this study has been described in detail previously (12), but is briefly summarized here for completeness. It consisted of six intensity modulated diode lasers and three continuous-wave diode lasers having wavelengths spanning from 660 nm to 850 nm (660 nm, 735 nm, 785 nm, 808 nm, 826 nm, 850 nm), and 900 nm to 950 nm (903 nm, 912 nm, 948 nm), respectively. Sixteen sequential source fiber positions

illuminated the breast, and the transmitted light was collected by an optical fiber pickup and sent to a rotating bank of photomultiplier tubes (PMT) and photodiode detectors. The NIRST data acquisition and computer control console resided in the MR control room but outside the MRI scanner bay, and long optical fiber bundles passed light to/from the NIRST instrument into the breast optical imaging interface attached to a standard commercial-grade breast MR coil unit (13).

A clinical MRI breast coil (Invivo Corp 800135) was retrofitted with the optical fiber imaging array that translates to accommodate variable breast sizes and compositions (13). During an examination, the fibers remained stationary and were mildly compressed against the breast surface in order to maintain contact. No significant degradation in the breast MRI image quality was evident due to the presence of the optical fibers. Figure 1 shows an overview of the NIRST system and integrated breast coil.

Measurement procedure

Subjects were fitted in a prone position into the optical breast interface in the MRI (MAGNETOM Trio 3.0T, Siemens) by lightly compressing three fiber optic cable holders against the breast. Co-registration between optical and MR images was accomplished through fiducial markers placed in the plane of each set of fibers. All patients underwent the same MRI protocol. Dedicated breast coils were used to acquire images with submillimeter in-plane resolution and section thicknesses of less than 3 mm (T1-weighted MR imaging) and less than 5 mm (T2-weighted MR imaging). MR sequences included diffusion-weighted imaging (DWI), T1-weighted DCE images, post-contrast axial, sagittal, and coronal multi-planar reconstruction (MPR), and signal intensity–time curves. The core dynamic scan was a three-dimensional (3D), fast, low-angle shot T1 sequence acquired in the transverse plane with a total of six acquisitions—one before and five after i.v. injection of MR contrast (0.5 mmol/mL, Gadodiamide, Omniscan, GE Healthcare) of 0.1 mmol per kilogram of body weight at 3 mL/s. Each volume consisted of 144 slices (1-mm thickness). The first post-contrast series was initiated 40 seconds after the injection. Subtraction images (gradient-echo T1-weighted precontrast series subtracted from initial post-contrast gradient-echo T1-weighted series) were generated at the MR workstation for either clinical or research examinations. The diffusion sequence was acquired using 8 b values ranging from 0 to 1,400 s/mm^2. Full tomographic optical data were collected at nine wavelengths concurrently with the MRI acquisitions and required 15 minutes relative to the 30-minute breast MRI examination.

Data analysis

Optical data were analyzed using NIRFAST, a custom optical image reconstruction software package written in Matlab (Math-works; ref. 14). Tissue regions were assigned to a patient-specific 3D finite element mesh based on the MR image volume segmented into adipose, fibroglandular, and abnormality regions (15). Data were calibrated based on a reference phantom to correct for variations in detector response and light intensity delivery. Images were reconstructed by minimizing the difference between measured data and a diffusion model of light propagation through the medium to yield estimates of the optical properties of the segmented tissue regions (16, 17). The image was formed via a Newton-type

minimization method that iteratively optimized the estimation of oxygenated and deoxygenated hemoglobin concentrations, water and lipid fractions, scatter amplitude, and scatter power in the predicted model based upon the measured data. Here, values of total hemoglobin, $HbT = HbO + Hb$, oxygen saturation, $StO_2 = HbO = HbT$; and a modified tissue optical index TOI = HbT * *Water/Lipid* were reported (3). After image reconstruction, contrasts between regions were evaluated rather than absolute values, as is common in many other imaging techniques (6). Each chromophore's ratio of tumor to normal tissue, based on the adipose region, was reported in subsequent analysis. The ratio of mean benign contrast to mean malignant contrast was also calculated for comparison with other analyses (3).

Statistical analysis

Patient examination results were divided into malignant ($n = 28$) and benign categories ($n = 16$) based on clinical pathology. Fourteen examinations were excluded from analysis because of insufficient coverage of the region of suspicion by the optical fiber array. Previous work (16, 18) has shown that optical image accuracy depends on having light signals that propagate through the abnormal region of interest with sufficient strength to be detected above the noise floor of the optical imaging array, and a measurement signal cutoff of 0.75% lesion sensitivity (relative to total sensitivity) was considered (10) as the minimum acceptable data sensitivity to the tissue region under evaluation. Based upon this analysis, data from 30 patient examinations met the signal sensitivity cutoff criterion, indicating that the breasts of these patients were accurately imaged across the plane of the tumor, and were subsequently evaluated.

MRI examinations were evaluated according to the Breast Imaging Reporting and Data System (BIRADS). Images were assessed based on morphologic features, DCE-MRI, and ADC values as references for detecting breast lesions. All malignant lesions were measured along three orthogonal axes, and the greatest diameter was considered in the statistical analysis. In cases of multifocal or multicentric cancer, only the largest lesion was evaluated. The dynamic and DWI scans were assessed at a dedicated workstation (Siemens Healthcare) where consensus was reached by two radiologists experienced in diagnostic breast MRI (J. Xu, 15 years, and K. Wang, 6 years), who were blinded to pathologic results. Images were evaluated based on the Teifke scoring system for focal breast lesions based on our previous experience and other results reported in the literature (19). Briefly, this system scores lesions based on shape, border characteristics, enhancement kinetics, and enhancement pattern and maps to a BIRADS category based on their cumulative scores (20, 21).

Statistical analysis was performed using Matlab. Student *t* tests and ROC analysis examined correlations between optical imaging and clinical pathology for all reconstructed optical parameters. *T* tests were performed using the Matlab "ttest2" algorithm. ROC analysis for MRI and individual optical chromophores was completed with respect to histolopathologic scoring on surgical samples. Coefficients to combine MRI and optical data were chosen using the Matlab "glmfit" function, which minimized the difference between the combined variable and pathologic analysis. ROC curves were drawn after this step and did not require further processing. Additionally, ROC data were tested using 1,000 trial permutation tests.

Significance for all statistical tests was assumed at a confidence interval of 95% ($P < 0.05$) for a two-tailed distribution.

Results

MRI interpretation

MRI were evaluated based on the BIRADS system by two radiologists experienced in breast MRI. The mean of the maximum dimension of the suspicious regions identified on the DCE-MRI examinations was 31 ± 19 mm, and ranged from 9 mm to 74 mm. Assuming a BIRADS 4 or 5 image rating to be positive for cancer, one false negative occurred out of the 21 pathologically confirmed malignant lesions, and 3 false positives resulted from the 9 benign cases, corresponding to a sensitivity and specificity of 95% and 67%, respectively. ROC analysis of MRI alone yielded an area under the curve of 0.87 (see Fig. 2).

Optical results

Quantification of normal tissue, abnormal tissue, and their ratio (abnormal/normal) for HbT and TOI is summarized in Fig. 2. Malignant lesions had statistically significant increases in HbT ($P < 0.01$) and TOI ($P < 0.001$), with mean contrast values of 1.09 ± 0.20 and 0.83 ± 0.27 for the malignant and benign cases in HbT, and 0.99 ± 0.34 and 0.69 ± 0.16 in TOI in the two diagnostic categories, respectively. The other optical parameters showed separation of means, but none were statistically significant (Fig. 2). The ratio of average malignant contrast and average benign contrast was 1.31 for HbT and 1.43 for TOI. At the given cutoff values, HbT had 0/21 false negatives and 6/9 false positives. TOI yielded 2/21 false negatives and 0/9 false positives. MRI combined with TOI yielded 1/21 false negatives and 1/9 false positives. Complete optical data from 30 analyzed patients can be found in Supplementary Table S1.

TOI was the best optical indicator and generated an AUC of 0.94, while the combination of TOI and MRI yielded an AUC of 0.95. HbT produced an AUC of 0.77 alone, and 0.89 when combined with MRI. Permutation tests on TOI, MRI, and TOI+MRI yielded permutation P <0.001, 0.001, and <0.001, respectively. Complete AUC, sensitivity, specificity, PPV, and NPV are summarized for the optical and combined indicators in Table 2.

Case examples

Two examples of MRI/NIRST examination data are highlighted in instances where the MRI diagnosis produced a false positive in Fig. 3. Patient 6 (pathology: fibroadenoma, BIRADS score: 4a) yielded HbT contrast of 0.32 and TOI contrast of 0.35 (Fig. 3A and B). Patient 10 (pathology: adenosis, BIRADS score: 4a) yielded HbT contrast of 0.62 and TOI contrast of 0.70 (Fig. 3C and D). Optical data correctly identified both of these lesions as benign.

Figure 4 shows a representative case example of MRI/NIRST examination data from a patient with a histologic cancer diagnosis. Patient 54 (pathology IDC, BIRADS score: 5) yielded HbT contrast of 1.58 and TOI contrast of 1.59. Optical data agreed with the true-positive MRI diagnosis and identified this lesion as malignant.

Discussion

MR-guided NIRST quantified HbT, StO_2, water and lipid content, and TOI in 30 women with undiagnosed breast abnormalities scheduled for surgical resection based on mammography, ultrasonography, or clinical examination. Histopathologic analysis of tissue removed during surgery identified 28 cancers and 16 benign lesions. Ratios of abnormal to normal tissue contrasts in these optical parameters were most predictive of malignancy, and were consistent with previous work (3, 6). Specifically, HbT and TOI were statistically significant indicators of malignancy ($P < 0.01$ and $P < 0.001$, respectively), similarly to findings in other optical breast imaging studies (22–24). However, the results presented here are the first to demonstrate improved diagnostic performance when these optical indicators are added to the MRI assessment of contrast-enhancing regions of interest (ROI) in a relatively large feasibility study of women with breast abnormalities of unknown diagnoses at the time of their imaging examinations. While the potential for diagnostic improvement in breast MRI through the incorporation of functional optical imaging parameters has been suggested in the past (2, 25), the anecdotal character of the prior results (less than 10 subjects imaged) has been augmented considerably by the much larger enrollments presented in this article.

MRI evaluation of the study data represents the interpretation of two experienced breast radiologists. Interestingly, ROC analysis of MRI alone yielded an AUC of 0.87, which is comparable to the values found in larger multicentered definitive studies of breast MRI (26) but lower than some single institution reports of particular patient populations or MRI scanning/analysis procedures (27–29), and could be due to sample size and/or the imbalance in the number of benign conditions in the enrollment group. Furthermore, the ROC analysis only provides an estimate of actual predictive performance because the data were evaluated in a training setting in terms of the instrumentation, algorithms, and imaging procedures. These results will need to be validated in a subsequent study to truly evaluate the diagnostic performance of the multimodality breast imaging approach.

Some MRI/NIRST examinations (14 in total) were excluded from the analysis based on a quantitative and objective assessment of the optical signal sampling of the MRI contrast-enhancing ROIs, which we attribute to the incomplete breast coverage that occurs with the current version of the optical imaging breast interface used in this study (10). The optical signal cutoff used to define an evaluable MRI/NIRST examination was based on its measurement sensitivity to the contrast-enhancing ROI because the optical measurements did not adequately interrogate the ROI in every case. Based on previous publications, inadequate optical data sensitivity depends on lesion location relative to optical fiber positioning and lesion size. Breast size and density also play a small role in determining the optical data sensitivity to the ROI, but they are secondary influences (10, 13). In this study, patients with insufficient optical measurement sensitivity to the suspicious ROI had breast cup sizes and densities distributed as 5 A-cup, 5 B-cup, 3 C-cup, and 1 D-cup sizes, and 3 fatty, 4 scattered, 4 heterogeneously dense, and 3 extremely dense parenchymal patterns, approximately in proportion to the totals in each group of enrollments. Providing full breast coverage is an important engineering challenge for future versions of the MRI/NIRST imaging array, and the positive diagnostic results reported here based on the analysis of 30

patient examinations with adequate optical signal sensitivity motivate a solution that economically maximizes breast coverage while still accommodating the majority of breast sizes (13).

In the two patient case studies presented, where MRI alone produced false positive results, both HbT and TOI correctly diagnosed the contrast-enhancing lesions as benign. Specifically, patient 6 (Fig. 3A and B) had HbT and TOI contrasts of 0.32 and 0.35, respectively, whereas patient 10 (Fig. 3C and D) had corresponding contrasts of 0.62 and 0.70. The case study presented in Fig. 4 shows representative MRI/NIRST examination data in a patient with histologically confirmed cancer. Patient 54 had HbT and TOI contrasts of 1.58 and 1.59. Malignancy contrast cutoffs of 0.94 and 0.88 for HbT and TOI, respectively, were used to generate the reported sensitivities and specificities (81% and 67% for HbT, 90% and 100% for TOI) in Table 2.

The results presented here appear to be an improvement over other studies with similar patient populations where combined optical and clinical imaging modalities were considered. For example, Poellinger and colleagues report an AUC of 0.796 for optical imaging combined with clinical mammography versus 0.722 for mammography alone in a study of 79 patients presenting with 42 malignancies (30). Previous work by Poplack and colleagues obtained an AUC of 0.67 for optical imaging alone in a group of 58 malignant lesions and 42 normal controls (6). Relative to previous publications, this study exploits the 3D high spatial and contrast resolution of MRI during optical image reconstruction to suggest improved diagnostic performance can be obtained, not only in terms of the optical parameters themselves, but, more importantly, in terms of the combined image information acquired by the multimodality technique (AUC 0.95 for MRI+TOI).

Optical biomarkers determined in this study were statistically significant indicators of breast malignancy and motivate further development of combined MRI/NIRST. The main limitation of the instrumentation was insufficient breast coverage, which led to the exclusion of 14 examinations due to lack of optical signal sensitivity to the ROI, and is readily addressed through redesign of the MRI/NIRST breast coil. Clinical translation of the technique is also not impeded by high cost, as the equipment required to add NIRST is nominal relative MRI, and comparable to state-of-the-art breast coil systems (<$100k, of which ~50% is for the optical fibers). Previous publications have suggested that the MRI/NIRST combination is compatible with clinical workflow (1, 14) and, certainly, could be optimized further. The results obtained from this study demonstrate synergy between NIRST and MRI, and represent a substantial advance toward clinical translation of the technique. This study supports and is consistent with trends toward the development and clinical use of multimodal imaging with systems such as PET/MRI, and, hopefully, will influence future work in the field. The molecular-specific information being added to MRI by simultaneous MRI/NIRST could lead to more informed and accurate biopsy decisions.

In the largest enrollment group reported to date (44 women, 30 analyzed), we show that improved diagnostic performance could occur when NIRST contrast in total hemoglobin concentration and tissue optical index in MRI contrast-enhancing regions of interest is added to the breast MRI assessment. These optical biomarkers were statistically significant

indicators of breast malignancy with abnormal to normal tissue contrasts comparable to those reported in previous studies. Importantly, adequate optical signal sampling of the contrast-enhancing lesions is critical to the success of the MR-guided NIRST image outcomes reported, and sufficient breast coverage was achieved in only about 70% of the examinations performed, which places a premium on the engineering challenges associated with new optical imaging array designs. Despite the imperfections in the optical imaging array applied in the present study, the very positive diagnostic outcomes from combined MRI/NIRST attained when sufficient optical coverage of the breast occurs, motivates the engineering effort required.

Supplementary Material

Refer to Web version on PubMed Central for supplementary material.

Acknowledgments

Grant Support

This work was funded by NIH grants R01 CA069544 and R01 CA132750.

References

1. Carpenter CM, Pogue BW, Jiang SJ, Dehghani H, Wang X, Paulsen KD, et al. Image-guided spectroscopy provides molecular specific information in vivo: MRI-guided spectroscopy of breast cancer hemoglobin, water, and scatterer size. Opt Lett. 2007; 32:933–5. [PubMed: 17375158]
2. Tromberg BJ, Pogue BW, Paulsen KD, Yodh AG, Boas DA, Cerussi AE. Assessing the future of diffuse optical imaging technologies for breast cancer management. Med Phys. 2008; 35:2443–51. [PubMed: 18649477]
3. Kukreti S, Cerussi AE, Tanamai W, Hsiang D, Tromberg BJ, Gratton E. Characterization of metabolic differences between benign and malignant tumors: high-spectral-resolution diffuse optical spectroscopy. Radiology. 2010; 254:277–84. [PubMed: 20032159]
4. Poellinger A, Burock S, Grosenick D, Hagen A, Ludemann L, Diekmann F, et al. Breast cancer: early- and late-fluorescence near-infrared imaging with indocyanine green–a preliminary study. Radiology. 2011; 258:409–16. [PubMed: 21177396]
5. Ntziachristos V, Yodh AG, Schnall MD, Chance B. MRI-guided diffuse optical spectroscopy of malignant and benign breast lesions. Neoplasia NYN. 2002; 4:347–54.
6. Poplack SP, Tosteson TD, Wells WA, Pogue BW, Meaney PM, Hartov A, et al. Electromagnetic breast imaging: results of a pilot study in women with abnormal mammograms. Radiology. 2007; 243:350–59. [PubMed: 17400760]
7. Pogue BW, Davis SC, Song X, Brooksby BA, Dehghani H, Paulsen KD. Image analysis methods for diffuse optical tomography. J Biomed Opt. 2006; 11:33001–16. [PubMed: 16822050]
8. Ntziachristos V, Yodh AG, Schnall M, Chance B. Concurrent MRI and diffuse optical tomography of breast after indocyanine green enhancement. Proc Natl Acad Sci U S A. 2000; 97:2767–72. [PubMed: 10706610]
9. Brooksby B, Pogue BW, Jiang S, Dehghani H, Srinivasan S, Kogel C, et al. Imaging breast adipose and fibroglandular tissue molecular signatures using hybrid MRI-guided near-infrared spectral tomography. Proc Nat Acad Sci USA. 2006; 103:8828–33. [PubMed: 16731633]
10. Mastanduno MA, Xu J, El-Ghussein F, Jiang S, Yin H, Zhao Y, et al. Sensitivity of MRI-guided near-infrared spectroscopy clinical breast exam data and its impact on diagnostic performance. Biomed Opt Express. 2014; 5:3103–15. [PubMed: 25401024]

11. Poplack SP, Paulsen KD, Hartov A, Meaney PM, Pogue BW, Tosteson TD, et al. Electromagnetic breast imaging: average tissue property values in women with negative clinical findings. Radiology. 2004; 231:571–80. [PubMed: 15128998]
12. El-Ghussein F, Mastanduno MA, Jiang S, Pogue BW, Paulsen KD. Hybrid photomultiplier tube and photodiode parallel detection array for wide-band optical spectroscopy of the breast guided by magnetic resonance imaging. J Biomed Opt. 2013; 19:11010–10.
13. Mastanduno MA, El-Ghussein F, Jiang S, DiFlorio-Alexander R, Junqing X, Hong Y, et al. Adaptable near-infrared spectroscopy fiber array for improved coupling to different breast sizes during clinical MRI. Acad Radiol. 2014; 21:141–50. [PubMed: 24439327]
14. Dehghani H, Eames ME, Yalavarthy PK, Davis SC, Srinivasan S, Carpenter CM, et al. Near infrared optical tomography using NIRFAST: Algorithm for numerical model and image reconstruction. Commun Numer Methods Eng. 2008; 25:711–32. [PubMed: 20182646]
15. Carpenter C, Srinivasan S, Pogue B, Paulsen K. Methodology development for three-dimensional MR-guided near infrared spectroscopy of breast tumors. Opt Express. 2008; 16:17903–14. [PubMed: 18958072]
16. Dehghani H, Pogue BW, Shudong J, Brooksby B, Paulsen KD. Three-dimensional optical tomography: resolution in small-object imaging. Appl Opt. 2003; 42:3117–28. [PubMed: 12790463]
17. Srinivasan S, Pogue BW, Jiang S, Dehghani H, Kogel C, Soho S, et al. In vivo hemoglobin and water concentrations, oxygen saturation, and scattering estimates from near-infrared breast tomography using spectral reconstruction. Acad Radiol. 2006; 13:195–202. [PubMed: 16428055]
18. Mastanduno MA, Jiang S, DiFlorio-Alexander R, Pogue BW, Paulsen KD. Remote positioning optical breast magnetic resonance coil for slice-selection during image-guided near-infrared spectroscopy of breast cancer. J Biomed Opt. 2011; 16:66001–8.
19. Qianxin, J. Application of 3.0T MR on breast imaging. Xi'an, China: The Fourth Military Medical University; 2008.
20. Teifke A, Lehr HA, Vomweg TW, Hlawatsch A, Thelen M. Outcome analysis and rational management of enhancing lesions incidentally detected on contrast-enhanced MRI of the breast. Am J Roentgenol. 2003; 181:655–62. [PubMed: 12933456]
21. Kuhl CK, Mielcareck P, Klaschik S, Leutner C, Wardelmann E, Gieseke J, et al. Dynamic breast MR imaging: Are signal intensity time course data useful for differential diagnosis of enhancing lesions? Radiology. 1999; 211:101–10. [PubMed: 10189459]
22. Cerussi A, Shah N, Hsiang D, Durkin A, Butler J, Tromberg BJ. In vivo absorption, scattering, and physiologic properties of 58 malignant breast tumors determined by broadband diffuse optical spectroscopy. J Biomed Opt. 2006; 11:44005–12.
23. Zhu Q, Hegde PU, Ricci A, Kane M, Cronin EB, Ardeshirpour Y, et al. Early-stage invasive breast cancers: potential role of optical tomography with US localization in assisting diagnosis. Radiology. 2010; 256:367–78. [PubMed: 20571122]
24. Chance B, Nioka S, Zhang J, Conant EF, Hwang E, Briest S, et al. Breast cancer detection based on incremental biochemical and physiological properties of breast cancers: a six-year, two-site study. Acad Radiol. 2005; 12:925–33. [PubMed: 16023383]
25. Pogue BW, Davis SC, Leblond F, Mastanduno MA, Dehghani H, Paulsen KD. Implicit and explicit prior information in near-infrared spectral imaging: accuracy, quantification and diagnostic value. Philos Trans R Soc Math Phys Eng Sci. 2011; 369:4531–57.
26. Bluemke DA, Gatsonis CA, Chen MH, DeAngelis GA, DeBruhl N, Harms S, et al. Magnetic resonance imaging of the breast prior to biopsy. J Am Med Assoc. 2004; 292:2735–42.
27. Kuhl CK, Jost P, Morakkabati N, Zivanovic O, Schild HH, Gieseke J. Contrast-enhanced MR imaging of the breast at 3.0 and 1.5 T in the same patients: initial experience. Radiology. 2006; 239:666–76. [PubMed: 16549623]
28. Lehman C, Isaacs C, Schnall M, Pisano E, Ascher S, Weatherall M, et al. Cancer yield of mammography, MR, and US in high-risk women: prospective multi-institution breast cancer screening study. Radiology. 2007; 244:381–8. [PubMed: 17641362]

29. El Khouli RH, Macura KJ, Jacobs MA, Khalil TH, Kamel IR, Dwyer A, et al. Dynamic contrast-enhanced MRI of the breast: quantitative method for kinetic curve type assessment. AJR Am J Roentgenol. 2009; 193:W295–W300. [PubMed: 19770298]

30. Poellinger A, Martin JC, Ponder SL, Freund T, Hamm B, Bick U, et al. Near-infrared laser computed tomography of the breast: first clinical experience. Acad Radiol. 2008; 15:1545–53. [PubMed: 19000871]

Translational Relevance

The results of this study suggest that MR-guided near infrared spectral tomography (NIRST) can distinguish malignant lesions from benign conditions in women with undiagnosed breast abnormalities via optical imaging biomarkers of total hemoglobin concentration and a tissue optical index. Functional information obtained from combined NIRST and clinical MRI could improve the diagnostic performance of dynamic contrast-enhanced MRI alone by adding molecular information and thereby improve patient care by reducing the number of unnecessary biopsies.

Figure 1.

An overview of the MRI/optical system. The optical system is housed in the MRI control room (A) and light is piped into the MRI suite for patient imaging using fiber optic cables (B). A combined MRI/optical breast coil (C) makes simultaneous MRI and optical imaging possible.

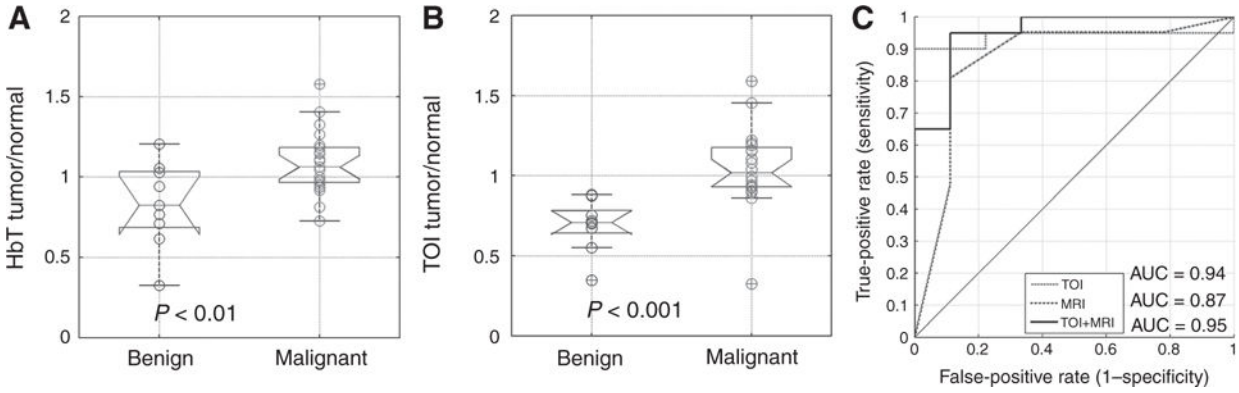

Figure 2.

Boxplots for optical parameters HbT (A) and TOI (B) for benign (n = 9) and malignant groups (n = 21). Significant differences occurred in the means of HbT and TOI. ROC analysis (C) of TOI, MRI, and combined MRI+TOI showed that MR-guided NIRST increases the AUC over standard DCE-MRI.

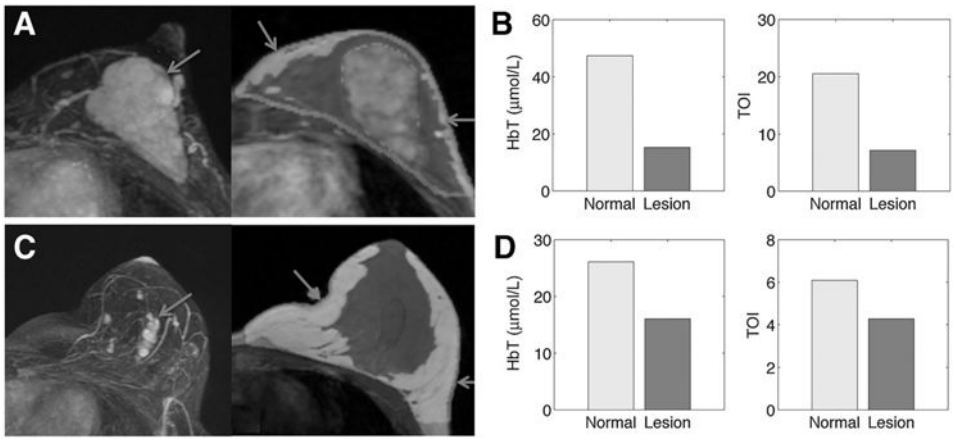

Figure 3.

MRI/optical results for patient 6 (lesion size: 48 × 53 × 22 mm, MRI: BIRADs 4a, path: adenosis) and patient 10 (lesion size: 10 × 20 × 19 mm, MRI: BIRADS 4a, path: fibroadenoma). Post-contrast MRI MIP images show abnormality location (left images of A and C) and enhancement pattern. MRI-based region maps (right images of A and C) segmented from T1 MRI were used to guide optical reconstruction. Arrows show locations of optical fibers. Graphs of HbT and TOI contrast correctly characterize the lesions as benign in both cases based on an ROI to normal contrast less than 0.94 and 0.88, respectively, are shown in B and D.

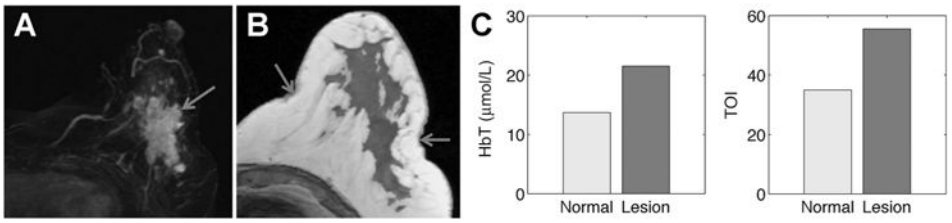

Figure 4.

MRI/optical results for patient 54 (lesion size: 20 × 59 × 40 mm, MRI: BIRADs 5, path: IDC). Post-contrast MRI MIP image shows abnormality location (A) and enhancement pattern. An MRI-based region map (B) segmented from T1 MRI was used to guide optical reconstruction and arrows show locations of optical fibers. C, Graphs of HbT and TOI contrast correctly characterize the lesion as malignant based on ROI to normal contrast greater than 0.94 and 0.88, respectively.

Table 1

Patient clinical information with tumor radiologic and pathology information as recorded

Classification	Age (y)	BMI (kg/cm^2)	Lesion size (mm)	US ACR BIRADS	Premenopausal	Postmenopausal
Cancer—28	49 (24–81)	23.7 (18.0–31.3)	31 (10–74)	4.6 (2–5)	15	13
Fibroadenoma—6	32 (20–51)	20.8 (18.7–25.5)	39 (21–81)	3.2 (2–4)	6	0
Adenosis—4	34 (23–48)	21.5 (18.1–25.0)	31 (13–53)	3.0 (3–4)	3	1
Other benign—6	42 (35–51)	23.1 (18.8–27.3)	28 (9–61)	3.5(2–5)	4	2

Table 2

Diagnostic performance of optical and combined indicators

30 Patients	HbT	TOI	MRI	MRI + HbT	MRI + TOI
AUC	0.77	0.94	0.86	0.89	0.95
Sensitivity	0.81	0.90	0.95	0.90	0.95
Specificity	0.67	1.00	0.67	0.89	0.89
PPV	85	82	87	95	95
NPV	60	100	86	80	89